JSER

Journal of Solar Energy Research (JSER)

Journal homepage: jser.ut.ac.ir

Investigating the effect of nano-structured magnetic particles lanthanum strontium manganite on perovskite solar cells

Mahsa Seifpanah sowmehsaraee[a], Maryam Ranjbar [*a], Mohammad Abedi[*a]

[a]*Department of Chemical Technologies, Iranian Research Organization for Science and Technology (IROST*), *P.O. Box 33535-111, Tehran, Iran*

Received: 2021-06-04
Accepted: 2021-10-25

Abstract

In this study, pure phase nanostructured strontium-doped lanthanum manganite, $La_{0.75}Sr_{0.25}MnO_3$ (LSM), with a hexagonal structure was synthesized by sonochemical method. Then, XRD and SEM estimated the size of the LSM nanopowders. The results are exhibited that products synthesized in this method are compatible with particle size and morphology. Magnetic measurement was done by vibrating sample measurement (VSM) on LSM nanoparticles at room temperature. According to the results obtained from VSM displayed the saturation magnetization of LSM nanoparticles exhibited a maximum of 24.25 emu/g at room temperature. Then, the influence of LSM nanoparticle as an additive on the film morphology of $CH_3NH_3PbI_3$ and the performance of perovskite solar cells was examined. We explore by using 5wt % of additive can increase the short current density (J_{sc}) from 14.45±0.55 to 18.29±0.38 mA/cm^2 (~ 26.5 % enhancement) and power-conversion efficiency (PCE) from 8.33±0.40 to 12.41±0.35 (~ 49 % enhancement). Moreover, the morphology, and band gap of the new perovskite layer was improved.

Keywords: Lanthanum strontium manganite, Perovskite, VSM, Solar cells, additive.

1. Introduction

Perovskite solar cell (PSCs) has received significant attention due to their suitable photovoltaic properties of perovskite layers are attributed to their excellent optoelectronic specifications, such as high absorption coefficient, low exciton binding energy, and tunable energy bandgap [1-4]. The good perovskite films can be provided using various methods such as sequential deposition [5], the one-step solution process [6], using anti-solvent during spin-coating [7], employing hot-substrate [8], and recently via adding additive [9]. Over the past few years, the incorporation of additives in the perovskite solution has become the most common method to improve film morphology and the crystallinity of perovskite. An assortment of additives in perovskite solar cells included polymer, fullerene, metal-halide salts, inorganic acids, solvent, organic halide salts, nanoparticle, etc [10]. For modifying the film quality, additive optimization was developed, which accelerates the crystallization process, thus producing remarkably smooth and uniform films of perovskite. Nevertheless, choosing a suitable additive is very important and essential. As mentioned, polymers are a typical class of additives used in PSCs. So far, polymers such as $[PbBr_2(C_9H_{15}N_5O)]_n$, nano-manganite, Cu/Zn/$Al_2O_3$-AC (AC = activated carbon), Zn(II) containing metal-organic frameworks, hybride perovskite, polythiophene, and

* E-mail: marandjbar@irost.ir

polythiocyanogen have been considered [11-18]. Strontium doped lanthanum manganite with perovskite structure can be used as an additive in perovskite solar cells because it is one of the proper materials used in solid oxide fuel cells (SOFCs) when the electrolyte is yttria zirconia [19]. SOFCs appear to be the most popular fuel cell technologies because it can directly convert into electrical energy by the electrochemical combination of hydrogen, and oxygen [20]. The cathode materials of SOFCs should have features such as having high electronic conductivity, stability in the air, thermal expansion coefficient, porous microstructure (porosity about 40 %) and chemical interaction with electrolyte should be minimum. Moreover, these features like electrical conductivity and porous morphology, should not change in the lifetime of the cells and the SOFCs process. LSM nanoparticle or Strontium doped lanthanum manganite is a perovskite material with *p*-type conductivity. Perovskite has a specific crystal structure with the ABX_3 formula (X=oxygen and halogen). The *p*-type conductivity of $LaMnO_3$ is due to the forming of cation vacancies and increased by substituting with a lower valence ion as a dopant like an alkaline field in A and, or B sites. The particle size of LSM nanoparticle with $La_{0.75}Sr_{0.25}MnO_3$ structure is suitable cathode material for high-temperature SOFCs. So far, various methods such as gel casting, solid-state reaction, solution combustion, microwave, sol-gel process, co-precipitation, aerosol pyrolysis, and sonochemical as a simple method used for the preparation of LSM nanoparticles, LSM films, and powders [13, 19, 21, 22].

In this study, sonochemical used for preparation of LSM nanoparticles. This method mainly used for the preparation of many nano-sized structures materials [12, 13, 23]. Then $La_{0.75}Sr_{0.25}MnO_3$ was used as an additive for investigation of its effect on morphology and structure of the $CH_3NH_3PbI_3$ film and its application in the perovskite solar cells. The influence of various amounts of $La_{0.75}Sr_{0.25}MnO_3$ on the surface morphology of perovskite films was revealed by scanning electron microscopy (SEM) and X-ray diffraction (XRD). Optimizing additive lead to the increase of power conversion efficiency (PCE), fill factor (FF) of perovskite solar cells. Here, we preferred the a one-step solution-process fabrication of perovskite by the solvent-engineering technique because it plays a significant role in characterizing the film quality. [7]

2. Materials and Methods

2.1. Materials and physical techniques

All of the chemical reagents for the synthesis of additive and analysis were commercially available from Merck company. They were used directly without purification. Materials for the fabrication of solar cells such as the TiO_2 paste, PbI_2, CH_3NH_3I, and spiro purchased from Sharif Solar Company. All materials for the synthesis of $CH_3NH_3PbI_3$ solution (in DMF&DMSO) for one-step spin-coating, and diethyl ether for solvent-engineering techniques purchased from Merck Co.For additive synthesis, the multiwave ultrasonic generator (Sonicator-4000; Misonix, USA), operating at 20 kHz with a maximum power output of 600 W, was employed. FT-IR spectrum was registered on a Bruker tensor 27 spectrophotometer by using of the KBr disk technique in the range 400–4000 cm^{-1}. Absorption spectra of the perovskite layers recorded by a Shimadzu UV-3103 UV–Vis spectrophotometer. The crystalline nature and phase purity examined using powder X-ray diffraction (XRD) technique (X'Pert Pro, INEL Equinox 3000, X-ray diffractometer) at room temperature with Cu-Kα (λ = 1.54 Å) radiation. The crystallite sizes of LSM nanoparticle and perovskite film calculated using the Scherrer formula. Tescan Mira FE-SEM and energy dispersive X-ray (EDX) instrument was used to study the surface morphology of LSM nanoparticle and perovskite films. Magnetization (M) as a function magnetic field (H) was measured for LSM nanoparticles in a vibrating sample magnetometer (VSM, BHV-55, Riken, Japan) at room temperature. Current-voltage (I-V) curves measured under simulated sunlight instrument, and air mass 1.5 G illumination (palmsens) Sharif Solar, Iran. Impedance spectroscopic measurements performed using an electrochemical workstation (Autolab 302N) with a frequency range from (100 kHz-100 mHz).

2.2. Preparation of nano-structured LSM by the sonochemical method

In a typical experiment, $La(NO_3)_3.6H_2O$, $Sr(NO_3)_2$ and $Mn(CH_3COO)_2.4H_2O$ with a stoichiometric ratio of 3:1:4 for preparation $La_{0.75}Sr_{0.25}MnO_3$ dissolved in distilled water. The optimal measure of NaOH solution (1.5 M) under sonication added into the primary solution until the pH reached ~8. The product centrifuged. In the following, product was washed with DI water to eliminate impurities, and dried in ambient air. The product suspended in ethanol under sonication for 10 min. Then, it dried at 100 °C for one h. After calcination in air with a heating rate of 5

˚C/min at 850˚C the black product (LSM nanoparticles) with magnetic properties achieved. Since the sonication time seems to effective in formation of the of LSM nanoparticles. So, in this experimental work, the maximum purity of LSM nanoparticles obtained in conditions of 30 min/60 ˚C (350 W) sonication. The results exhibited that via the sonochemical method, the formation time is decreased. In contrast, at a high calcination temperature of 850 ˚C with a heating rate of 5 ˚C/min resulted in the spherical LSM nanoparticles with an average size of about 69.

2.3 Device fabrication

Fluorine-doped Tin Oxide (FTO) with (15 G/square) coated glass substrates were cut into 1.5 cm × 1.5 cm sizes. For the preparation of the half-cell, one piece of FTO glass was etched by Zn powder in 6 M HCl solution, then was cleaned by sonication in acetone, dilute solution of HCl, ethanol, isopropyl alcohol, and DI water for 10 min each, followed by annealing at 500 ºC for one hour. To form a thick TiO_2 blocking layer, diluted titanium isopropoxide solution in ethanol, spin-casted (1000 r.p.m, 30 sec) onto FTO substrated. They were followed by annealing at 500 °C for one hour. A mesoporous TiO_2 layer (m-TiO_2) was deposited by spin coating for (4000 r.p.m, 20 sec). The substrate was immediately and quickly annealed at 100 °C for 10 min, in the following sintered at 450 °C for 30 min. Perovskite precursor with $CH_3NH_3PbI_3$ formula obtained by 462 mg PbI_2, and 159 mg CH_3NH_3I in 1ml mixed solvent of DMF: DMSO= 4:1 (volume ratio), with solvent engineering techniques were deposited by spin–coating (4500 r.p.m, 30 sec). During spin-coating, diethyl ether (150 µL) [7] was poured on the spinning substrate each 12 seconds [24]. Then, the substrated annealed at 100 ºC for 10 min. Subsequently, the hole transport layer, Spiro-MeOTAD, was deposited by spin-coating (3000 r.p.m, 30 sec). Finally, Au was evaporated on the top of the perovskite to produce a completed PSC device.

3. Results & Discussion

3.1 Characterization of LSM nanoparticle prepared via the sonochemical method

Fig. 1 shows a schematic of the technique employed for the preparation of nano-structured LSM perovskite. The vibration in the infrared spectrum (FT-IR spectra) of the LSM nanoparticle prepared via the sonochemical method is shown in the frequency range from 400 to 4000cm^{-1} is illustrates in Fig. 2. The leading absorption bands around 606 and 489 cm^{-1} for $La_{0.75}Sr_{0.25}MnO_3$ can be attributed to stretching of the metal-oxygen bond in the perovskite. This can be due to the internal motion of a change in Mn–O–Mn bond length in MnO_6 octahedral [25]. The bands position is in good agreement with the previous paper [26]. These results prove the formation of the perovskite LSM is compatible with the XRD data (see Fig. 3).

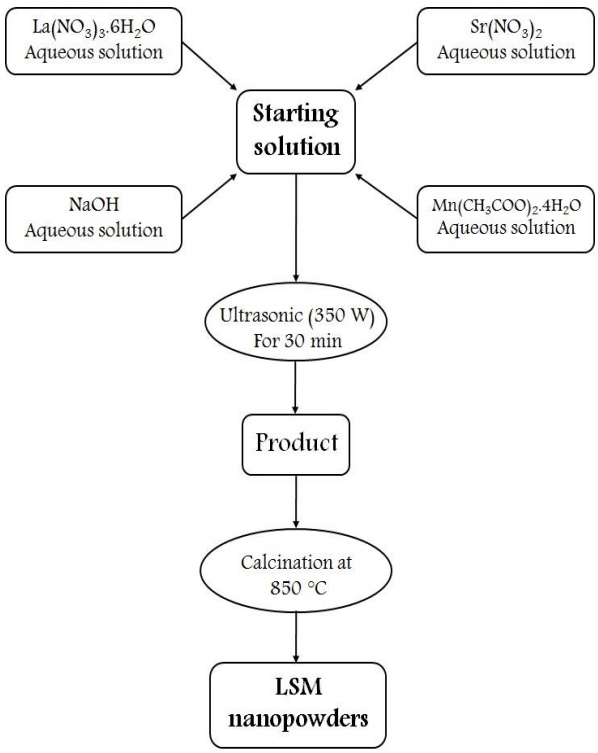

Figure 1. Schematic representation of LSM nanopowders.

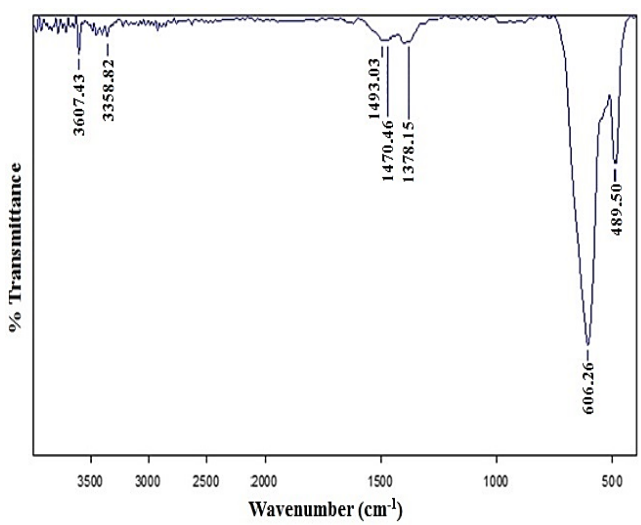

Figure 2. FT-IR spectrum of LSM nanoparticles.

Fig. 3. exhibits the XRD pattern of LSM powder obtained after calcination at 850˚C under air atmosphere. Simulated XRD pattern displayed the existence of perovskite phase $La_{0.75}Sr_{0.25}MnO_3$ with the hexagonal symmetry (JCPDS card no.: 056-0616) (see Fig. 3). Moreover, this XRD pattern compared with the standard diffraction pattern indicates no peaks of impurities. Besides, the presence of sharp diffraction peaks suggests the product is crystalline, and the presence of broadening peaks indicates that the particle is of nanometer scale. Scherrer formula utilized to calculate the particle size by simulated XRD pattern.

$$d = \frac{(0.891\ \lambda)}{cos\theta_B\ .\ [(B^2_{sample} - B^2_{reference})^{0.5}]}$$

In Eq. (1), d is the crystallite size, β is the full width at half maximum (FWHM) of diffraction peak in radians, λ is the wavelength, and θ is diffraction angle [13]. The lattice parameters, and average crystallite size of the product have been shown in Table 1, which is in good agreement with the previous literature. [21]

from FESEM. These results are compatible with the everage size of XRD data. The EDX spectrum shows the presence of lanthanum, strontium, and manganese as the only elementary components. This is good

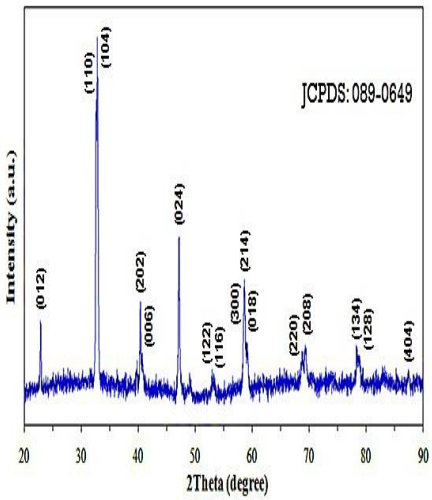

Figure 3. XRD pattern of LSM nanoparticles prepared via sonochemical method.

Fig. 4 exhibits FESEM micrograph and EDX analysis of products synthesized via the sonochemical method in this work. The results demonstrate the product obtained by this method is uniform particles with proper size distribution. Besides, that spherical-shaped morphology is evidence for the existence of nanoparticles. Table 1 shows the average size of LSM evidence that the synthesized product is in proper stoichiometry, and no impurity peak was observed in the EDX.

Table 1. Lattice parameters and size for nano perovskite-type oxide, LSM synthesized using sonochemical method.

Lattice constant (Å)			Cell volume V (Å^3)	Average size (nm)	
a	*b*	*c*		XRD	FESEM
5.516	-	13.329	350.592	75	69

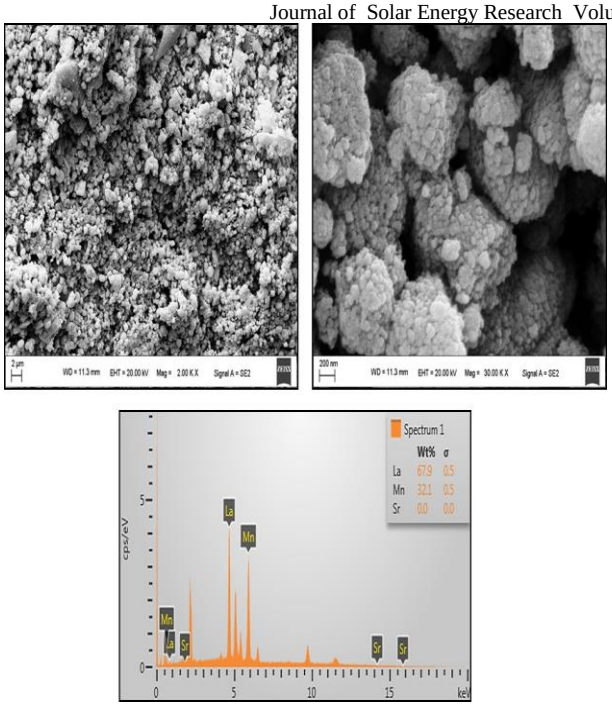

Figure 4. FESEM photographs and EDX analysis of LSM nanoparticles prepared via sonochemical method**.**

Fig. 5 shows the room temperature magnetization curve of the LSM nanoparticle. A vibrating sample measurement (VSM) was used to measure the magnetic properties of LSM. As the result, which showed typical ferromagnetic behavior at room temperature. Simultaneously, a finite coercivity of 310.5 O_e was present at 300 K (see Fig. 5). The results exhibited the amount of saturation of the final product (24.25 emu/g) is remarkably much less than that reported for the multidomain bulk particle (71 emu/g). The decrease in saturation magnetization adapted in terms of non-collinear spin arrangement the surface of the particle at or near in the range 10-100 nm. On the other hand, at room temperature, the magnetic hysteresis measured exhibits the product has low ferromagnetic properties.

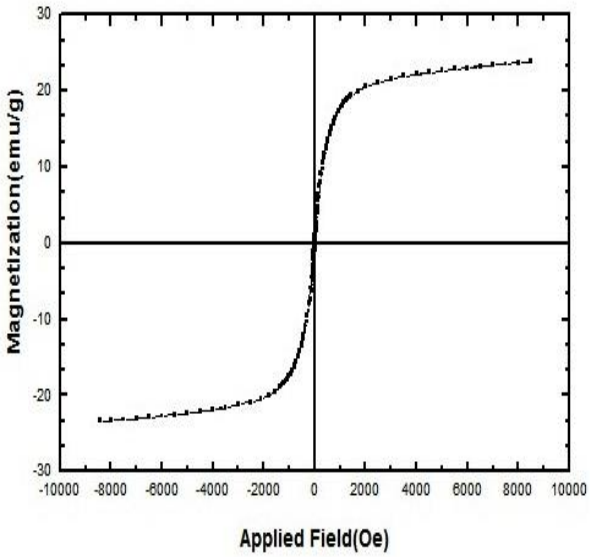

Figure 5. M-H curve for LSM nanoparticles prepared by ultrasonic irradiation at room temperature.

3.2 Characterization of perovskite solar cells

We synthesized LSM nanoparticles prepared via the sonochemical method. This research, mostly focused on the effect of LSM nanoparticles with different percentages in perovskite film and devices, and their roles in film morphology, light absorption, and device performance were discussed. To examine the effect of LSM nanoparticles synthesized on performance of PSCs. At the beginning of the work, $CH_3NH_3PbI_3$ solutions ($CH_3NH_3PbI_3$ in DMF and DMSO) with different amounts of LSM nanoparticles (0- 2.5- 5-10 wt%) prepared and used for fabrication of PSCs. We employed LSM nanoparticle by a solvent-engineering technique in a one-step deposition of solution ($CH_3NH_3PbI_3$ with LSM nanoparticle in DMF&DMSO) to fabricate perovskite layer. The performance of perovskite solar cells based on $CH_3NH_3PbI_3$ with different amounts of LSM nanoparticles are shown in Fig. 6 and Table 2. The results show the solar cell with 5% of LSM nanoparticles has the highest short-circuit current density (J_{sc}) and power conversion efficiency (PCE), while in the cell without additive (pristine) has the lower open-circuit voltage (V_{oc}) and fill factor (FF). Moreover, in cells with 10% of LSM nanoparticle caused the reduction of short current density (J_{sc}), and open-circuit voltage (V_{oc}), and PCE. As a result, by adding 10 wt% of LSM nanoparticle, which causes the formation of many voids, that led to the phase separation of during the perovskite crystal formation. Thus the J_{sc} and PCE are decreased. Moreover, the hysteresis of J-V curves was examined. In general, it can be seen that the presence of additives can reduce the hysteresis, and increase the fill factor. The effect of additives on the perovskite solution is also crucial.

Specifically, the interaction between metals and oxygen with iodide could passivate the surface perovskite film, and performance of PSCs.

Table 2. I-V characteristics of the fabricated LSM nanoparticles-based PSCs.

No	LSM in perovskite precursor solution	[1] J_{sc} [mA/cm^2]	[2] V_{oc} [V]	[3] FF	[4] η [%]
I	0.0 wt% of additive	14.45±0.55	0.99±0.03	0.58±0.12	8.3±0.4
II	2.5wt% of additive	15.51±0.64	1.03±0.01	0.69±0.10	11.1±0.3
III	5.0 wt% of additive	18.29±0.38	1.01±0.02	0.67±0.09	12.4±0.3
IV	10.0 wt % of additive	13.52±0.43	0.99±0.04	0.59±0.55	7.94±0.5

[1] J_{SC} (mA cm^{-2}) is the short-circuit current density.
[2] V_{OC} (V) is the open-circuit voltage.
[3] FF is the fill factor.
[4] η (%) = $(J_{SC} \times V_{OC} \times FF)/P_{in}$ where P_{in} is the incident light.

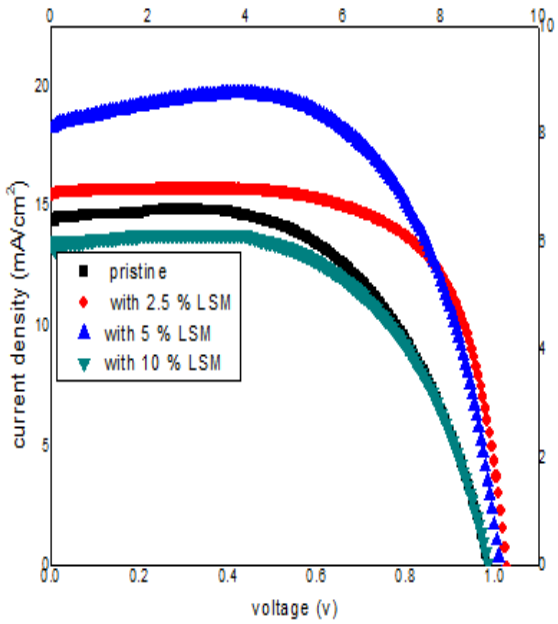

Figure 6. J-V curves of $CH_3NH_3PbI_3$ PSC devices with or without additive measured under illumination of an AM 1.5 solar simulator (100 mW cm^{-2}) in air, and the scanning direction is from open-circuit voltage to short circuit.

Figure 7a,b,c,d represents the $CH_3NH_3PbI_3$ top-view SEM images with (0- 2.5- 5-10 wt%) of LSM nanoparticles. In Fig.7a (pristine), 7b (2.5% wt of additive), 7c (5% wt of additive), and 7d (10% wt of additive) exhibit one phase with different intensity of some peaks. The pristine $CH_3NH_3PbI_3$ layers were prepared by a one-step spin-coating method, with anti-solvent Diethyl ether was dripped on the FTO/TiO_2-block/ TiO_2–mp substrate during spinning. Some layers, including 2.5, 5, 10 wt% of LSM nanoparticle, were employed to investigate the influence of additives on the perovskite film quality. Figure 7c illustrates top-view SEM images of perovskite films, with 5% of the LSM nanoparticle. As shown in figure 7(a) to 7(c), the surface morphology of perovskite film with 5 % LSM nanoparticle is regular and without pinholes and uniform coverage than pristine film. When the amount of LSM nanoparticles was increased from 5% to 10 %, lead to perovskite layer with smaller grain size, and numerous pinholes created. Consequently, the SEM images disclosed that the compact $CH_3NH_3PbI_3$ film with uniform coverage could be achieved plainly by optimal the amount of additive. So, The LSM additive into $CH_3NH_3PbI_3$ by an one-step solution method plays a key role in morphology and crystal structure of perovskite film. This phenomenon is essential for the photovoltaic capacity of the corresponding cell. Figure (7e), and (7f) EDX analysis of perovskite layers clearly shows the existence of strontium-doped lanthanum manganite in perovskite layers and confirms the presence of elements of LSM nanoparticle

.

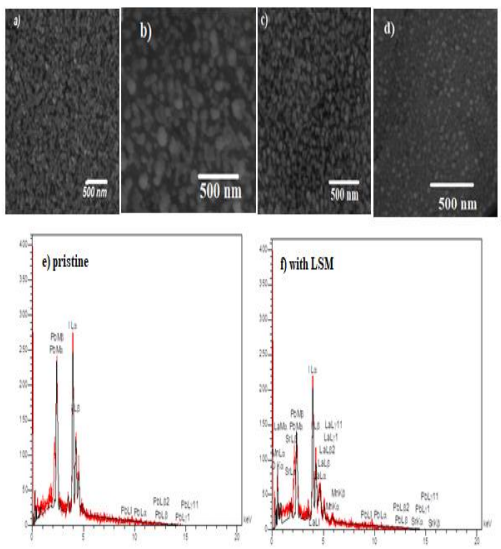

Figure 7. FESEM micrograph of the a) $CH_3NH_3PbI_3$ without additive (pristine perovskite film), b) with 2.5 % wt of additive c) with 5 % wt of additive d) with 10 % wt of additive and EDX analysis of e) pristine perovskite layer f) perovskite layer with additive

Figure 8 shows XRD patterns of the $CH_3NH_3PbI_3$ films to check the effect of additives on morphology and crystallinity after adding the different amounts of LSM nanoparticles. After adding (0- 2.5- 5-10 wt%) of additives, all XRD peaks located at 2θ value of 14.2º, 19.9º, 24.5º, 26.5º, 31.8º, and 40.6º that indicated the prepared films have a tetragonal crystal structure. Thus, despite different amount of the LSM nanoparticle, perovskite was effectively formed. For more study of the layers, X-ray diffraction (XRD) was used to measure the crystal sizes of perovskite layers, with the Sherrer equation [27]. By assuming the most intense peaks at 2θ=14.2 the average crystalline size of perovskite layer was estimated. The calculated crystallite size showed the sizes 61.3 nm (for pristine), 48.8 nm (for 2.5 wt %), 48.3 nm (for 5

wt %), and 45.6 nm (for 10 wt %) of LSM nanoparticles as an additive in the perovskite layers. It means that, under the same condition, the $CH_3NH_3PbI_3$ film with LSM nanoparticle as additives have more nucleation density and small crystals. As can be seen, there is more coverage of $CH_3NH_3PbI_3$ film [28]. Moreover, in figure 8, for films which without additive, shows a peak at 12.6° related to PbI_2 (001), which indicate partial decomposition or remaining unreacted PbI_2 in perovskite film [29]. As the result, by adding more the amounts of LSM nanoparticles the intensity of PbI_2 peak decrease. Until, in the perovskite layer, which contains 5 and 10 % of LSM nanoparticle, this peak disappears completely. It is evident from figure 8(c) and 8(d) the presence of LSM nanoparticle shows a positive effect on the stability of perovskite layer.

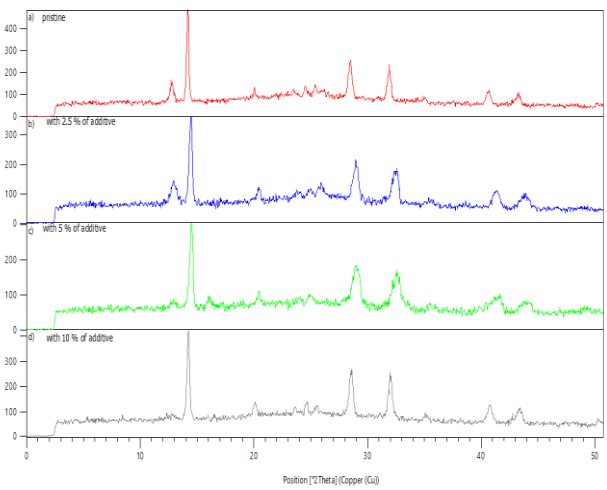

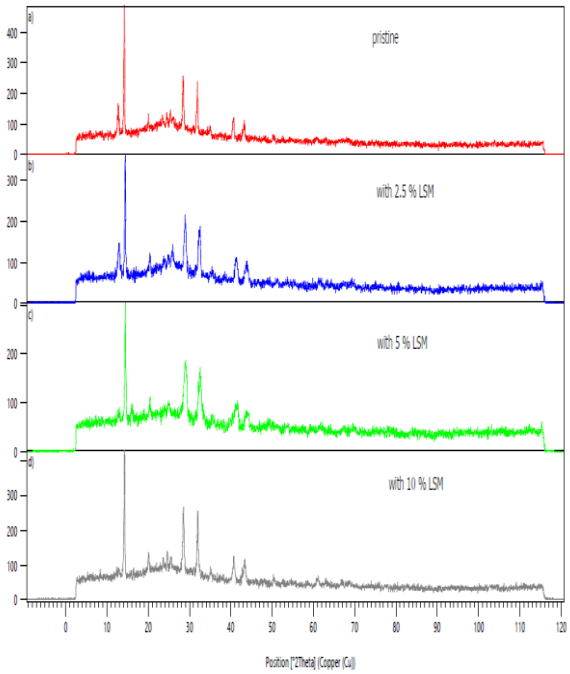

Figure 8. The X-ray powder diffraction pattern of a) $CH_3NH_3PbI_3$ film without additive (pristine perovskite film), b) with 2.5 % wt of additive, c) with 5 % wt of additive, and d) with 10 % wt of additive

We employed UV-Vis absorption spectroscopy to determine the absorption range and intensity of perovskite films (show figure 9). The absorption shows the excitation peak between 400 to 450 nm, and the onset of absorption is in the range of 700-800 nm. The perovskite precursors fabricated with 5% LSM nanoparticles presented higher absorption than others. Which has consisted of SEM result indicating. The light absorption of perovskite film with 10 wt% of LSM nanoparticles is lowest, maybe due to the inhomogeneity and decreasing the quality of resulting perovskite film. These results confirmed with corresponding Jsc and PCE in Table 2 and XRD in Figure 8.

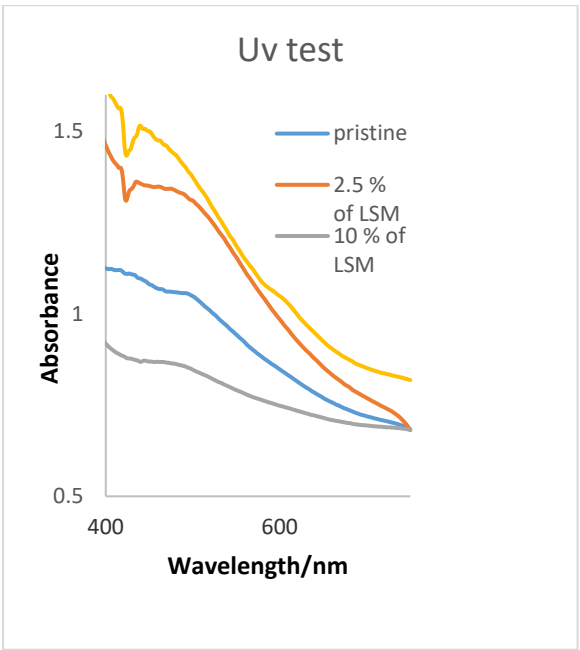

Figure 9. UV-vis absorption spectra of a) pristine perovskite film b) with 2.5 % wt of additive, c) with 5 % wt of additive, and d) with 10 % wt of additive

UV-Vis absorption was also used to check the band gap. According to that, the amount of band gap for pristine, and with LSM, 1.68- 1.88 were obtained respectively (see figure 10). Therefore, due to the presence of lanthanum, Manganese and stranthium metals, the band gap is increased. This calculation was performed with the Tauck relation.

$(\alpha h\nu)=B(h\nu - Eg)^{\frac{n}{2}}$ (2)

In this formula, α is absorption coefficient, B is constant absorption, hν is Stimulation energy, Eg is Band gap energy, and n is constant number which is one for direct transfer, and four for indirect transfer. Absorption coefficient was calculated using the following formula.

$\alpha=2/0303 \times 10^{3} \left(\frac{AP}{LC}\right)$ (3)

In this formula, α is absorption coefficient, L is optical path length, A is sample adsorption amount in UV-Vis, C is sample molar concentration, and *P* is density [30, 31].

a)

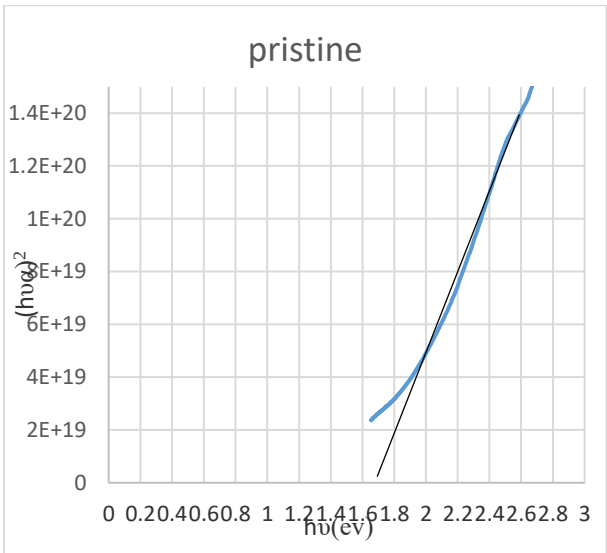

b)

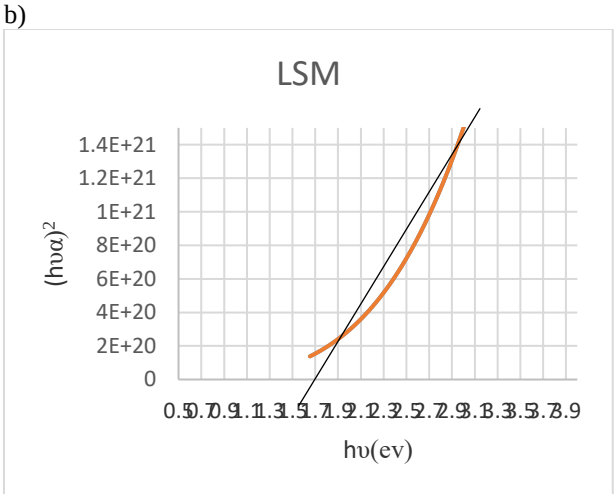

Figure 10. Band gap comparation of a) pristine perovskite film b) with LSM

Figure 11 shows the Nyquist plots of perovskite with and without additives under AM1.5 sun illumination. The resistance decrease for additive compares then without additive or pristine. It indicated the defects in perovskite film were reduced by adding additives,

thus leading to better cell performance and less recombination.

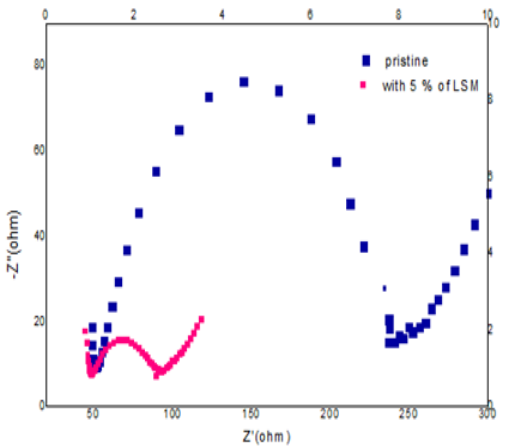

Figure 11. Nyquist plots of the layers with and without additives

4. Conclusions

In conclusion, nano-structured strontium-doped lanthanum manganite, $La_{0.75}Sr_{0.25}MnO_3$ (LSM), were prepared via sonochemical methods because of this method compared to other ways does not need high temperature during the reaction, and it is swift. The product characterized through FT-IR, XRD, FESEM and EDX. The simulated XRD pattern shows only the one phase, and pattern assigned to perovskite-type of LSM that crystallizes in a hexagonal structure. EDX analysis reveals the presence of lanthanum, strontium, and manganese as the only elementary components. For more investigation, VSM analysis was used. We found the saturation magnetization for smaller crystals had a lower value than the bulk value. Then, LSM nanoparticles was used as an additive in perovskite solar cells. By using 5wt % of LSM nanoparticles was increased the short current density (J_{sc}) from 14.45±0.55 to 18.29±0.38 mA/cm^2 and power-conversion efficiency (PCE) from 8.33±0.40 to 12.41±0.35. Moreover, the band gap of the new perovskite layer was studied by UV-Vis. As a result, LSM nanoparticle improves the coverage of perovskite film on the TiO_2 layer and it can help to the stability of perovskite solar cells.

Acknowledgements

The authors are grateful to the Iranian Research Organization for Science and Technology (IROST).

References

[1] De Wolf, S., Holovsky, J., Moon, S.J., Löper, P., Niesen, B., Ledinsky, M., Haug, F.J., Yum, J.H. and Ballif, C., Organometallic halide perovskites: sharp optical absorption edge and its relation to photovoltaic performance. *The journal of physical chemistry letters*, 2014. *5*: p.1035-1039.

[2] Eperon, G.E., Stranks, S.D., Menelaou, C., Johnston, M.B., Herz, L.M. and Snaith, H.J., Supplementary information Formamidinium of Formamidinium lead trihalide: a broadly tunable perovskite for efficient planar heterojunction solar cells. *Energy Environ. Sci*, 2014. *7*: p.982.

[3] Kagan, C.R., Mitzi, D.B. and Dimitrakopoulos, C.D., Organic-inorganic hybrid materials as semiconducting channels in thin-film field-effect transistors. *Science*, 1999.*286*:p.945-947.

[4] Stranks, S.D., Eperon, G.E., Grancini, G., Menelaou, C. and Alcocer, M., JP; Leijtens, T.; Herz, LM; Petrozza, A.; Snaith, HJ Electron-Hole Diffusion Lengths Exceeding 1 Micrometer in an Organometal Trihalide Perovskite Absorber. *Science*, 2013. *342*:p.341-344.

[5] Burschka, J., Pellet, N., Moon, S.J., Humphry-Baker, R., Gao, P., Nazeeruddin, M.K. and Grätzel, M., 2013. Sequential deposition as a route to high-performance perovskite-sensitized solar cells. *Nature*, 2013. *499*: p.316-319.

[6] Xiao, M., Huang, F., Huang, W., Dkhissi, Y., Zhu, Y., Etheridge, J., Gray-Weale, A., Bach, U., Cheng, Y.B. and Spiccia, L., A fast deposition-crystallization procedure for highly efficient lead iodide perovskite thin-film solar cells. *Angewandte Chemie International Edition*, 2014. *53*:p.9898-9903.

[7] Jeon, N.J., Lee, J., Noh, J.H., Nazeeruddin, M.K., Gratzel, M. and Seok, S.I., Efficient inorganic–organic hybrid perovskite solar cells based on pyrene arylamine derivatives as hole-transporting materials. *Journal of the American Chemical Society*, 2013. *135*:p.19087-19090.

[8] Nie, W., Tsai, H., Asadpour, R. and Blancon, J., C., Neukirch AJ, Gupta G., Crochet JJ, Chhowalla M., Tretiak S., Alam MA, Wang H.-L., Mohite AD. 2015. *Science*, *347*: p.522.

[9] Liang, P.W., Liao, C.Y., Chueh, C.C., Zuo, F., Williams, S.T., Xin, X.K., Lin, J. and Jen, A.K.Y., 2014. Additive enhanced crystallization of solution-processed perovskite for highly efficient planar-heterojunction solar cells. *Advanced materials*, 2014. *26*:p.3748-3754.

[10] Li, T., Pan, Y., Wang, Z., Xia, Y., Chen, Y. and

Huang, W., 2017. Additive engineering for highly efficient organic–inorganic halide perovskite solar cells: recent advances and perspectives. *Journal of Materials Chemistry A*, 2017. *5*: p.12602-12652.

[11] Ranjbar, M., Çelik, Ö., Najafi, S.H.M., Sheshmani, S. and Mobarakeh, N.A., Synthesis of lead (II) minoxidil coordination polymer: a new precursor for lead (II) oxide and lead (II) hydroxyl bromide. *Journal of Inorganic and Organometallic Polymers and Materials*, 2012. *22*: p.837-844.

[12] Ranjbar, M. and Yousefi, M., Synthesis and characterization of lanthanum oxide nanoparticles from thermolysis of nano-sized lanthanum (III) supramolecule as a novel precursor. *Journal of Inorganic and Organometallic Polymers and Materials*,2014. *24*:p.652-655.

[13] Yousefi, M. and Ranjbar, M., Ultrasound and Microwave-Assisted Co-precipitation Synthesis of La 0.75 Sr 0.25 MnO 3 Perovskite Nanoparticles from a New Lanthanum (III) Coordination Polymer Precursor. *Journal of Inorganic and Organometallic Polymers and Materials*, 2017. *27*:p.633-640.

[14] Dehghani, A., Ranjbar, M. and Eliassi, A., Modification of Cu/Zn/Al $_2$ O $_3$ catalyst by activated carbon based metal organic frameworks as precursor for hydrogen production. *Journal of Inorganic and Organometallic Polymers and Materials*, 2018. *28*:p.585-593.

[15] Seifpanah Sowmehesaraee, M., Ranjbar, M., Abedi, M., Rouhani, F. and Morsali, A., The Effect of Zn (II) Containing Metal-Organic Frameworks on Perovskite Solar Cells. *Progress in Color, Colorants and Coatings*, 2020.*14*:p.259-267.

[16] Choudhary, S., Shukla, A., Chaudhary, J. and Verma, A.S., 2020. Extensive investigation of structural, electronic, optical, and thermoelectric properties of hybrid perovskite ($CH_3NH_3PbBr_3$) with mechanical stability constants. *International Journal of Energy Research*,2020. *44*: p.11614-11628.

[17] Luqman, M., Ghiat, I., Maroof, M., Lahlou, F.Z., Bicer, Y. and Al-Ansari, T., 2020. Application of the concept of a renewable energy based-polygeneration system for sustainable thermal desalination process—A thermodynamics' perspective. *International Journal of Energy Research*, *44*(15), pp.12344-12362.

[18] Kahani, S.A., Maleki, E. and Ranjbar, M., Investigating the effect of polythiocyanogen on morphology and stability of the perovskite layer and its application in the hole-transport material free perovskite solar cell. *Journal of Photochemistry and Photobiology A: Chemistry*, 2020.*389*: p.112218.

[19] Im, J., Park, I. and Shin, D., Preparation of nano-crystalline strontium-doped lanthanum manganate (LSM) powder and porous film by aerosol flame deposition. *Ceramics International*, 2014. *40*:p.5567-5573.

[20] Kakade, M.B., Ramanathan, S., Dey, G.K. and Das, D., Processing and characterisation of porous lanthanum strontium manganite–role of porosity on electrical conductivity and morphology. *Advances in applied ceramics*, 2008. *107*:p.89-95.

[21] Deml, A.M., Stevanović, V., Holder, A.M., Sanders, M., O'Hayre, R. and Musgrave, C.B., Tunable Oxygen Vacancy Formation Energetics in the Complex Perovskite Oxide Sr x La1–x Mn y Al1–y O3. *Chemistry of Materials*, 2014. *26*:p.6595-6602.

[22] Tarragó, D.P., de Fraga Malfatti, C. and de Sousa, V.C., Influence of fuel on morphology of LSM powders obtained by solution combustion synthesis. *Powder Technology*, 2015. *269*: p.481-487.

[23] Ranjbar, M. and Yousefi, M., 2016. Sonochemical synthesis and characterization of a nano-sized lead (II) coordination polymer; a new precursor for the preparation of PbO nanoparticles, 2016.12:p.109-118.

[24] Maleki, E., Ranjbar, M. and Kahani, S.A.,. The effect of antisolvent dropping delay time on the morphology and structure of the perovskite layer in the hole transport material free perovskite solar cells. *Progress in Color, Colorants and Coatings*, 2021. *14*: p.47-54.

[25] Maleki, E., Ranjbar, M. and Kahani, S.A., The effect of antisolvent dropping delay time on the morphology and structure of the perovskite layer in the hole transport material free perovskite solar cells. *Progress in Color, Colorants and Coatings*, 2021.*14*:p.47-54.

[26] Abdel-Latif, I.A., Ismail, A.A., Bouzid, H. and Al-Hajry, A., Synthesis of novel perovskite crystal structure phase of strontium doped rare earth manganites using sol gel method. *Journal of Magnetism and Magnetic Materials*, 2015. *393*: p.233-238.

[27] Zhang, W., Saliba, M., Moore, D.T., Pathak, S.K., Hörantner, M.T., Stergiopoulos, T., Stranks, S.D., Eperon, G.E., Alexander-Webber, J.A., Abate, A. and Sadhanala, A., Ultrasmooth organic–inorganic perovskite thin-film formation and crystallization for efficient planar heterojunction

solar cells. *Nature communications*, 2015. *6*:p.1-10.
[28] Wu, Y., Islam, A., Yang, X., Qin, C., Liu, J., Zhang, K., Peng, W. and Han, L., Retarding the crystallization of PbI 2 for highly reproducible planar-structured perovskite solar cells via sequential deposition. *Energy & Environmental Science*, 2014. *7*:p.2934-2938.
[29] Guo, X., McCleese, C., Kolodziej, C., Samia, A.C., Zhao, Y. and Burda, C., Identification and characterization of the intermediate phase in hybrid organic–inorganic MAPbI 3 perovskite. *Dalton Transactions*, 2016. *45*:p.3806-3813.
[30] Makuła, P., Pacia, M. and Macyk, W., How to correctly determine the band gap energy of modified semiconductor photocatalysts based on UV–Vis spectra, 2018:p.6814-6817.
[31] Jubu, P.R., Yam, F.K., Igba, V.M. and Beh, K.P., 2020. Tauc-plot scale and extrapolation effect on bandgap estimation from UV–vis–NIR data–a case study of β-Ga2O3. *Journal of Solid State Chemistry*,2020. *290*: p.121576.